LANGMUIR

Article

pubs.acs.org/Langmuir

Templated $CaCO_3$ Crystallization by Submicrometer and Nanosized Fibers

Andrónico Neira-Carrillo,[*,†,‡] Rafael Gentsch,[§] Hans G. Börner,[∥] Diego Fernando Acevedo,[⊥] Cesar Alfredo Barbero,[⊥] and Helmut Cölfen[#]

[†]Faculty of Veterinary and Animal Sciences and [‡]Advanced Center for Chronic Diseases (ACCDiS), University of Chile. Av. Santa Rosa 11735, Santiago, Chile

[§]Evonik Corporation, Birmingham, Alabama 35211, United States

[∥]Department of Chemistry, Humboldt-Universität zu Berlin, Brook-Taylor-Str. 2, 12489 Berlin, Germany

[⊥]Department of Chemistry, Universidad Nacional de Río Cuarto, Córdoba, Argentina

[#]Physical Chemistry, Department of Chemistry, University of Konstanz, 78457 Konstanz, Germany

Supporting Information

ABSTRACT: Electrospun submicrometer-sized poly(ε-caprolactone) (PCL) meshes and nanosized multiwalled carbon nanotubes (MWCNTs) were used as a template for preparing porous and interconnected inorganic−organic hybrid materials composed of $CaCO_3$. Herein, we describe the proportion and incorporation method of submicrometer-sized plasma-treated PCL meshes over areas >1 mm^2 with $CaCO_3$ using three crystallization methods including the use of poly(acrylic acid) (PAA). We found that flexible and rigid acid-functionalized MWCNTs showed a clear capacity and effects to penetrate calcite particles. MWCNTs interacted differently with the individual growth planes of $CaCO_3$, indicating that fibers can undergo changes depending on sulfonate or carboxylate groups, adopt different orientations in solution, and thereby elicit changes in $CaCO_3$ morphology. In summary, the use of PCL and acidic MWCNT fibers as an additive for substrate templates and experimental crystallization provides a viable approach for studying various aspects of biomineralization, including the production of controlled particles, control of porosities, and defined morphologies at microscale and nanoscale levels.

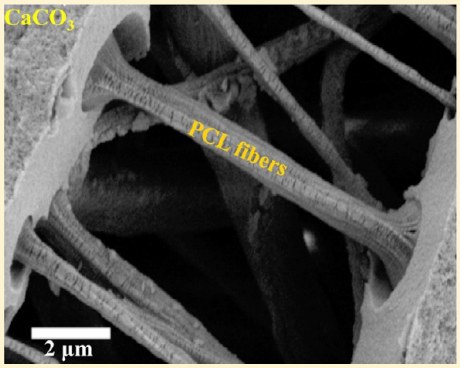

INTRODUCTION

Biomineralization is the process by which living organisms ranging from higher vertebrates and plants to unicellular organisms produce hierarchical inorganic−organic hybrid biominerals.[1−3] Representative examples of biominerals are bones and teeth in vertebrates, shells in molluscs, exoskeletons in crustaceans, coccoliths in marine algae, plant opals in higher plants, and magnetite in bacteria, among others.[2−7] Biominerals play crucial roles in living organisms such as protection, motion, storage, optical and gravity sensing, defense, and detoxification.[6−9] They are highly organized from the molecular to the nanoscale and macroscale, with intricate nanoarchitectures that ultimately make up myriad different functional soft and hard tissues[1,9−11] These nanostructured hybrid biominerals present a complex shape, hierarchical organization, uniform particle size, and novel morphologies that often have high strength and remarkable properties. Therefore, chemists are inspired by the underlying molecular processes and aim to mimic biological crystallization to transfer the concepts to modern composite materials and the control of mineral crystallization. The toughness of biominerals depends on the degree of crystallization, soluble and/or insoluble polymer matrices, the shape (platelet, fibers, etc.), and the type of inorganic minerals.[2,7,12,13]

It is well known that biominerals are valuable materials not only for understanding the biomineralization concepts but also for novel confined-materials synthesis and design, avoiding undesirable pathological biomineralization.[14,15] The inspiration from biomineralization and nanocomposite materials that control crystal nucleation and growth is of great interest to materials scientists who seek novel materials syntheses with fibrillar hydrogel structures and/or crystalline matrices and interfaces based on crystalline forms analogous to those produced by nature, such as calcium salts, silica, hydroxyapatite, or iron oxides.[16−21]

The current work discusses the selection and use of calcium carbonate ($CaCO_3$) as a biologically relevant system. $CaCO_3$ has three anhydrous polymorphs: calcite (trigonal), aragonite (orthorhombic), and vaterite (hexagonal). This biomineral often consists of single crystals intimately associated with macromolecular organic matrices. Calcite is one of the most common biomineral phases.[22−25] Because of its biocompatible and biodegradable nature, encapsulation, and drug delivery capacity, strong interest for pharmaceutical and biomedical applications

Received: July 9, 2016
Revised: August 16, 2016
Published: August 16, 2016

DOI: 10.1021/acs.langmuir.6b02536
Langmuir 2016, 32, 8951−8959

has also emerged. Recently, hybrid nanoparticles of the $CaCO_3$–polyaniline biomaterial as a photothermal agent for cancer ablation were demonstrated as a new platform for the next generation of in vivo cancer photothermal therapy agents.[26]

The aim of this study was to design hybrid composite materials using electrospun submicrometer-sized PCL meshes and nanosized MWCNTs as templates for preparing porous and interconnected organic–inorganic hybrid materials composed of $CaCO_3$. Template-directed mineralization as strategy has become one of the most popular methods for preparing hybrid composite materials.[27] Templated synthesis is an exciting area of research capable of producing highly controlled nanostructures with unique structures, morphologies, and advanced properties.[28] Therefore, the understanding of bioinspired directed mineralization mechanisms, charge/polarization matching, epitaxy based on $CaCO_3$ using different nanomaterial assemblies as a template, and the growth induction of inorganic materials has been extensively investigated.[29]

The fiber-enhanced composite materials have the pores fully filled by the organic phase that modulates the mechanics of the inorganic crystals by analogy to occluded proteins or micelles.[30−32] Such composite structures have multiple potential applications in the technical field as well as in the medical field (e.g., 3D scaffolding).[33] Regarding the architecture, the present approach can be considered, to some extent, to be like a steel-reinforced concrete construct. In addition, the first report of bioinspired crystallization of $CaCO_3$ on electrospun cellulose acetate submicrometer fibers as a scaffold by Yu et al. demonstrated the viability of an organic–inorganic material interface.[34] In this context, CNTs represent versatile materials with novel properties, making them potentially useful in many applications such as nanotechnology, electronics, optics, and other fields of materials science. While CNTs could be incorporated into mineral crystals, raw CNTs appear as insoluble bundles of several fibers held together by Π–Π interactions. Covalent functionalization could introduce bulky groups, which weaken the interactions, separate the nanotubes, and form interactions with the solvent, allowing the dispersion of the materials. Several methods have been proposed to functionalize CNTs.[35,36] Among them, the coupling of highly reactive aromatic radicals, produced by the thermal decomposition of diazonium salts, with CNTs is an easy way to produce water-dispersible CNT systems.[37] Here, we have used the method to synthesize different covalently functionalized MWCNTs that show clear effects on calcite particle mineralization.[38] Previously, dispersed CNTs have been used to produce composites with hydroxyapatite crystals.[39−41]

In summary, this article explores a bioinspired approach of templating from the nanoscale to the microscale using electrospun fiber meshes composed of submicrometer and nanometer PCLs and MWCNTs as templates to obtain integrated porous crystal–fiber interface nanomaterials.

MATERIALS AND METHODS

Materials. Poly(ε-caprolactone) (PCL, Sigma-Aldrich) was reprecipitated prior to use.[42] Chloroform ($CHCl_3$, 99+%, Merck, Darmstadt, Germany), methanol, tetrahydrofuran (THF), and *N*,*N*-dimethylformamide (DMF, 99+%, Sigma-Aldrich, Steinheim, Germany), were used as received. For aqueous solutions, bidistilled water was used (0.055 μS/cm, 23.4 °C). All salts used for crystallization were obtained from Sigma-Aldrich (high purity grade, Steinheim, Germany). $CaCO_3$ powder (99+%), calcium chloride ($CaCl_2$) dihydrate (96%) from (Sigma-Aldrich), ethanol, and ammonium carbonate were obtained from ACS-Merck and used without further purification. MWCNTs, produced by CVD growth from acetylene, were obtained from Sun Nanotech (China). The material was washed with 6 M HCl for 24 h to clean out metal contamination.

Diazonium Ion Synthesis and Covalent Modification of Carbon Nanotubes. Multiwalled CNTs (CNT, Sun Nanotech) were modified by coupling with aromatic radical cations, produced by the thermal decomposition of diazonium ions.[43] Aromatic amines were diazotized with sodium nitrite and concentrated HCl in an ice bath.[44] Diazotized amines were mixed with MWCNTs in an ultrasonic bath. Then, the temperature was raised to 60 °C and heated for 1 h. The reaction mixture was acidified with concentrated HCl and centrifuged (10 000 rpm) to separate the modified CNT. The precipitate was washed several times with water and dried under vacuum. Raw or functionalized CNT were dispersed in purified water with the aid of ultrasound. Dynamic light scattering (DLS) measurements were performed in a Malvern 4700 DLS. The measurements were made at an angle of 90° at 25 °C. As shown before,[43] the CNTs functionalized in such a way render a monomodal dispersion (Figure S.I.1) that is stable for months whereas raw CNTs show clusters of different sizes and precipitate spontaneously after a few minutes.

Electrospinning Setup. PCL solutions were prepared by dissolving the polymer overnight by mixing with a rock and roll shaker using THF/DMF (1:1). The electrospinning setup was composed of a setup described in previous work.[42] Plastic 1 mL syringes with disposable blunted tips (Howard Electronics, JG20-2, nominal inner diameter 0.584 mm, El Dorado, KS, USA) were positively charged, and an aluminum foil was used as the collector in a vertical setup. The polymer solution was fed at a rate of 1 mL/h by the syringe pump to the blunted needle tip, where a voltage of 15 kV was applied. The spinning distance between the tip and ground collector was 10 cm. The resulting fiber meshes were dried, cut into 0.5 × 0.5 cm^2 pieces, and sputtered with Pd/Au for SEM observation (LEO 1550-GEMINI, Zeiss, Oberkochen, Germany). To evaluate the fiber diameter, ImageJ softward (1.38x, Wayne Rasband, National Institutes of Health, Bethesda, MD, USA) was used. Wide-angle X-ray scattering (WAXS) of the PCL and PCL/composites was conducted on a PDS 120 diffractometer (Nonius GmbH, Solingen, Germany) with Cu Kα radiation.

Microscopy. In the case of CNT fibers and gas diffusion (GD) crystallization, both SEM and light microscopy (LM) measurements of $CaCO_3$ were applied to all crystal samples. The use of the LM was necessary to prove that the SEM micrographs show real structures instead of drying artifacts resulting from the sample preparation. SEM of $CaCO_3$ crystals was performed on a LEO 1550-GEMINI (Zeiss, Oberkochen, Germany) instrument. Additionally, LM images were taken with a VHX digital microscope (Keyence VH-Z1000).

Crystallization Methods. *$CaCO_3$ Crystallization with Electrospun Submicrometer PCL Fibers.* For crystallization, submicrometer-sized fibers of 0.2–1.2 μm diameter were used.[42] A self-sustained fiber mesh of ~0.8 × 0.8 cm^2 was used for the different crystallization methods. Air plasma treatment of the mesh was performed for 1 min using an 18 W PDC-32G plasma cleaner (Harrick Plasma, Ithaca, NY, USA). The concentrations of the respective $CaCl_2$, Na_2CO_3, and PAA solutions can be seen in Table 1, as can the solution volume and mineralization time. After mineralization, the composites were dried in air for corresponding analytics. For SEM, sputtering was performed with crystallization samples. Here, $CaCO_3$ powder was dissolved in an acidic aqueous solution (saturated at pH 3.6, adjusted with HCl), and then its pH was shifted to neutral conditions (pH 7, NaOH).

$CaCO_3$ Crystallization with CNT Fibers. The crystallization of $CaCO_3$ was based on the gas diffusion (GD) method. The diffusion of CO_2 into different concentrations (5, 10, and 25 mM) of an aqueous solution of $CaCl_2$ in the presence of acidic CNT fibers (10 wt %) as an additive was performed, and then $CaCO_3$ was slowly precipitated. The crystallization of $CaCO_3$ was carried out in closed desiccators at room temperature. GD crystallization was performed using raw multiwalled (CNT-1) and functionalized sulfonic (CNT-2, CNT-3) and carboxylic (CNT-5) CNT fibers at 20 °C for 2 and 5 days. The GD method was performed as we described in previous work.[45−49] The pH is very important in the biomineralization field. In the gas diffusion method, $CaCO_3$ crystallization is performed at a defined mineralization time,

DOI: 10.1021/acs.langmuir.6b02536
Langmuir 2016, 32, 8951−8959

Table 1. Different Conditions of $CaCO_3$ Mineralization[a]

methods	solution concentration	time	volume
gas diffusion (GD)	10 mM CC	3 days	~10 mL
GD, no plasma	10 mM CC	3 days	~10 mL
GD	25 mM CC, 50 mM PAA	1 day	~10 mL
GD	25 mM CC, 50 mM PAA	3.5 days	~10 mL
GD	25 mM CC, 50 mM PAA	1 week	~10 mL
double diffusion (DD)	10 mM CC and NC	2 days	~30 mL
DD, no plasma	10 mM CC and NC	6.5 days	~30 mL
DD	2.3 mM CC and NC	2 weeks	~30 mL
DD[16]	0.02 mM CC and NC, cooled at 4 °C	8 days	~30 mL
vacuum-assisted[15]	8 mM CC and NC	1 min	~0.5 mL
vacuum-assisted[15]	16 mM CC and NC	1 min	~0.5 mL
vacuum-assisted[15]	0.1 M CC, NC and PAA	20 min	~0.5 mL
centrifugation[18]	0.1 M CC, NC and PAA	60 min	~0.5 mL

[a]CC, $CaCl_2$ solution; NC, Na_2CO_3 solution; PAA, poly(acrylic acid) solution; no plasma, PCL fibers were not plasma-treated.

and the effect of pH is eliminated by fixing the pH using TRIS buffer at pH 9.0. After mineralization, the $CaCO_3$ crystals were rinsed with bidistilled water, dehydrated in a 50 to 100% gradient ethanol solution, dried at room temperature, and observed. CNT fibers in the desired quantity were added to the $CaCl_2$ solutions under stirring to ensure complete dissolution to obtain a $CaCl_2$ solution with the CNT additive. Then, equal volume $CaCl_2$ solutions (10 mL) were added to glass bottles with a volume of 12 mL. The bottles were covered with Parafilm, with three pinholes to allow diffusion of NH_3 and CO_2, and placed in a desiccator. Microscope coverslips (5−8 mm diameter) were placed in the $CaCl_2$ solutions (at the bottom of the bottles) to simplify the recovery of the crystals for microscopy. Finally, two glass bottles (10 mL) of crushed $(NH_4)_2CO_3$ were also covered with Parafilm, punched with three needle holes, and put at the bottom of the desiccator. After the mineralization reaction had taken place, the crystals were recovered, briefly washed with water, and allowed to dry. After gold coating, the crystals were examined with a scanning electron microscope. It is important to mention that all glassware (glass bottle and small pieces of glass substrate) was cleaned and sonicated in ethanol for 5 min and rinsed with bidistilled water and the filter was soaked in a H_2O−HNO_3 (65%)−H_2O_2 (1:1:1, v/v/v) solution. Then the glassware was rinsed with bidistilled water and finally dried in air with acetone. Additionally, a stock aqueous solution of $CaCl_2$ at different concentrations was freshly prepared in boiled bidistilled water and bubbled with N_2 for 2 h before use. Typical rhombohedral calcite crystals were obtained in the absence of fiber additives, whereas CNT additives selectively yield truncated and interpenetrated $CaCO_3$ crystals.

RESULTS AND DISCUSSION

Nonwoven meshes composed of submicrometer-sized PCL fibers[42] and nanosized MWCNTs are used as templates for crystallization processes to facilitate the generation of fiber-enhanced or -directed $CaCO_3$ composites as well as porous crystalline materials potentially with bimodal pore systems as shown schematically in Figure 1. The task here was to fully embed nanometer- and submicrometer-sized templates within $CaCO_3$ crystals. The fibers could then be removed by means of calcination or leaching. Porous crystals would be attractive for electronic, optical, sensory, or drug delivery applications, whereas a knowledge of molecular mechanisms of conformational changes on the microstructure of $CaCO_3$ composite hybrid materials could be interesting for controlling mechanical, medical, and optical applications. An ultrastructural investigation between organic and inorganic layers of hybrid composite materials is necessary, and surface properties, transport mechanisms of $CaCO_3$ nanoparticles, and the quantitative conformation change in organic molecules observed by atomic force microscopy (AFM) can be addressed.[50,51]

To effectively fill the pores of the PCL meshes, different crystallization routes have been explored. Direct crystallization methods were conducted in the first attempts, and amorphous calcium carbonate (ACC)-mediated pathways were performed in a second set of experiments. The latter were inspired by biomineralization in nature where ACC is believed to play an important role as a precursor form.[52,53] The meshes were mineralized by means of gas and double ion diffusion, precipitation, centrifugation, and vacuum-assisted infiltration with a transient ACC phase (Table 1).[54,55]

As a starting point, the GD method was employed where a plasma untreated submicrometer fibrous PCL mesh in an aqueous solution of 10 mM $CaCl_2$ was crystallized in a vessel by the decomposition of $(NH_4)_2CO_3$ into CO_2, H_2O, and NH_3. Most of the resulting crystals did not show the inclusion of fibers, but they rather expelled and lifted the fibers onto their top surface as visible in the Supporting Information (Figure S.I.2). To improve the interaction between $CaCO_3$ crystals and PCL fibers during crystallization, the fiber scaffold was plasma-activated (1 min, air, 18 W). During treatment, the ester bonds on the fiber surface are supposed to be cleaved and reacted with hydroxyl, carbonyl, and carboxyl groups.[15] In addition, the fiber mesh would be instantaneously wetted similarly to surface-functionalized fibers in contrast to the superhydrophobic behavior of untreated fibers.[56,57] Plasma-treated fibers were increasingly integrated into the calcite crystals as shown in Figure 2. However, the crystals seemed to grow from the fiber mesh rather than inside the fiber mesh. Attempts to switch the top side of the fiber mesh upside down after 1 day of crystallization in order to promote the ingrowth of crystals into the fiber mat were not successful.

To improve the limited integration of $CaCO_3$ into the fiber mesh, a double ion diffusion (DD) experiment was conducted.

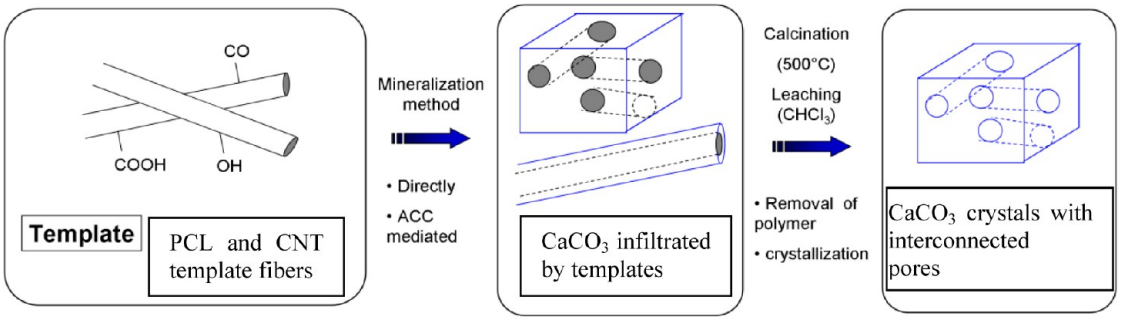

Figure 1. Schematic representation of $CaCO_3$/PCL and $CaCO_3$/CNT composites or porous $CaCO_3$ crystals by electrospun poly(ε-caprolactone) and CNT fibers.

DOI: 10.1021/acs.langmuir.6b02536
Langmuir 2016, 32, 8951−8959

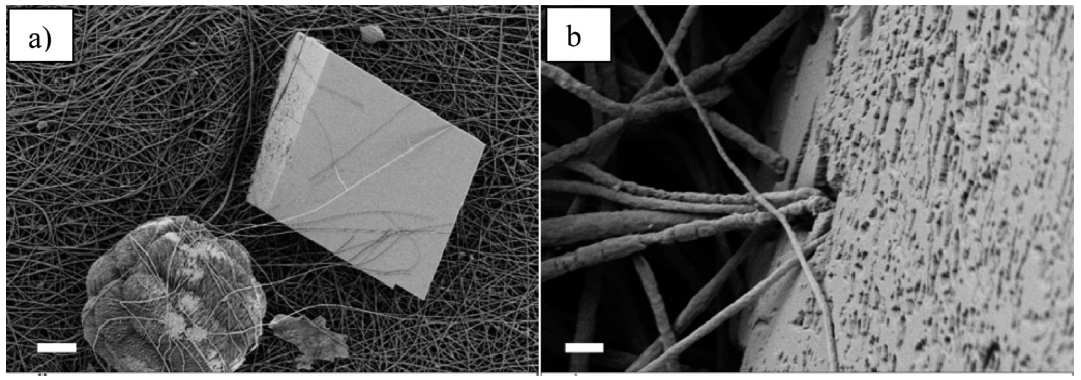

Figure 2. SEM images of $CaCO_3$ crystals revealed an improved interaction of plasma-treated PCL submicrometer-sized fibers by means of GD. Conditions: $CaCl_2$ = 10 mM, 3 days. Plasma: 1 min, 18 W. Scale bars: (a) 20 μm and (b) 1 μm.

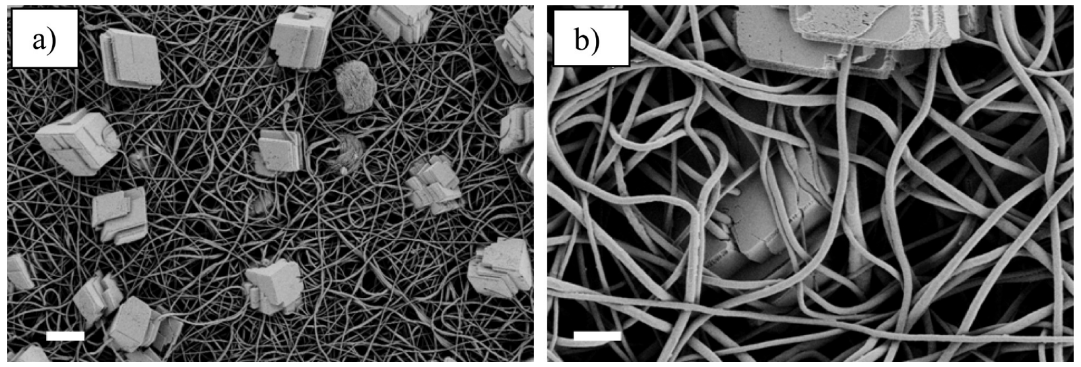

Figure 3. SEM images indicate that some $CaCO_3$ crystals were fully incorporated into the fiber mesh whereas others were still on the surface by means of double-diffusion crystallization. Conditions: $CaCl_2$ and Na_2CO_3 = 10 mM, 2 days. Scale bars: (a) 20 μm and (b) 5 μm.

The mesh was placed between two half U-tube arms, which were simultaneously filled with aqueous solutions of $CaCl_2$ and Na_2CO_3 (10 mM each). This procedure clearly improved the $CaCO_3$ incorporation, as can be seen from fully fiber-penetrated calcite crystals shown in Figure 3. Nonetheless, there seems to be a larger number of small crystals compared to those formed during the GD method. This suggests many nucleation points. In addition, there were still some crystals growing from the surface of the meshes. Experiments using plasma-untreated PCL and the variation of both concentrations and reaction times did not change the results dramatically.

Theoretically, the ideal case would be one nucleation point in the middle of the fiber mesh leading to a large single crystal. Practically, this is time-consuming because low supersaturation and hydrophobic surfaces are typically needed to prevent many heterogeneous nucleation sites. However, this might be bypassed using ACC intermediates inspired by nature. By this means, the pores might be filled with a liquidlike ACC, which converts directly into a crystal, or by the introduction of a second crystallization step as shown by Qi et al.[58] In addition, Meldrum et al. showed that the ACC stability could be increased by cooling the anion/cation solutions prior to the start of crystallization.[59] This was applied in a DD experiment; however, the results did not improve the situation shown in Figure 3. The concept of cooling solutions in advance was also applied to a vacuum-assisted method adapted from Qi et al.[58] This procedure was applied to a plasma-treated submicrometer-sized PCL mesh. Cooled aqueous $CaCl_2$ and Na_2CO_3 solutions were mixed to obtain a translucent phase that then served as an infiltration solution for the fiber mesh upon applying vacuum. Figure 4 summarizes the results using two solutions of different concentrations.

A final solution containing 8 mM $[Ca^{2+}]$ and $[CO_3^{2-}]$ ions (Figure 4a) resulted in small calcite-like structures after drying. Decreasing the concentration to 4 mM (Figure 4b) led to a large (200 × 500 μm^2) incorporation of likely amorphous $CaCO_3$ into the fiber mat. The WAXS pattern from the latter composite structure indicated no peak for crystalline $CaCO_3$ (Figure 5). The visible peaks were attributed to the semicrystalline orthorhombic PCL.[55] The lack of a crystalline peak might be an indication of ACC, which is in agreement with the liquid-like morphology of the $CaCO_3$. However, a low mineral content could be an alternative explanation.

To further increase the inorganic mass ratio in the composite, a method adapted from Kato et al. was applied.[60] A paste was generated by mixing an aqueous solution containing $CaCl_2$ and PAA with an aqueous Na_2CO_3 solution, reaching a concentration of 50 mM of each component in the final mixture. By aging and subsequent centrifugation of the resulting precipitate into the fiber mesh, deposition was mainly observed on the mesh surface (see Figure S.I. 3 in the Supporting Information). In contrast, using vacuum-assisted infiltration succeeded in the incorporation of fibers within the dried $CaCO_3$ crust as evident in a cross section of the film in Figure 6. The $CaCO_3$ film was probably broken by drying or handling. Nonetheless, the production of the large-scale (>1 mm^2) incorporation of PCL fibers was accomplished. The $CaCO_3$ film itself consisted of small particulates (Figure 6b) that might be composed of ACC as suggested by Kato et al.[60]

To verify the composite structure, WAXS was performed. No crystalline peak, which could be assigned to $CaCO_3$, was observed in the diffractogram. This suggests an amorphous form of $CaCO_3$ and is in agreement with the observations made by

DOI: 10.1021/acs.langmuir.6b02536
Langmuir 2016, 32, 8951−8959

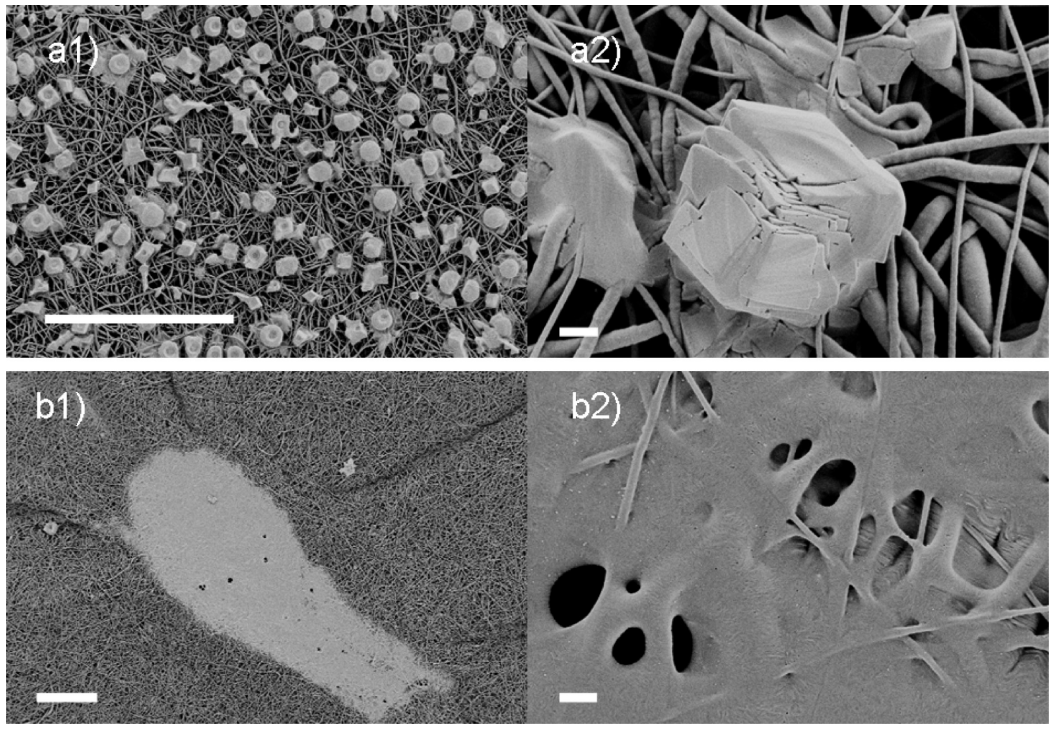

Figure 4. SEM images of PCL fiber meshes infiltrated by ACC precursor solutions. The incorporation of $CaCO_3$ was conducted by a vacuum-assisted protocol. (a) 16 mM or (b) 8 mM solutions of $CaCl_2$ and Na_2CO_3 were mixed, and then ~0.5 mL of the mixture was sucked into the mesh within ~1 min. Scale bars: (a1, a2) 100 μm and (b1, b2) = 2 μm.

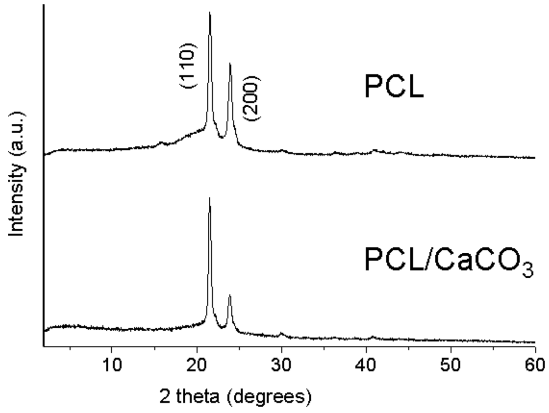

Figure 5. Wide-angle X-ray diffraction pattern of $CaCO_3$ on the fiber mesh indicating no crystalline peak attributed to $CaCO_3$.

Kato et al., who reported the stability of the ACC for at least 200 days under ambient conditions.[60] Overall, this method was feasible for coating a large mesh area within a short period of time.

Finally, a novel approach of combining the PAA concept as an ACC stabilizer with the GD method was applied. A solution of 25 mM $CaCl_2$ and 50 mM PAA was employed so that potentially every Ca^{2+} ion could be coordinated by a CO_3^{2-} group of PAA. The resulting composites can be seen in Figure 7. The inorganic composition could be gradually increased by the crystallization time. Whereas after 1 day only partial coating was achieved, crystallization proceeded in particle-like precipitates, which partially coated the entire fiber and mesh surface after 4.5 days (Figure 7b,d). In Figure 7d, it can be seen that some of the ACC particles transformed into calcite polycrystals. After 1 week, large areas (>1 mm^2) were coated as shown in Figure 7c. However, prolonging the mineralization time did not lead to the complete

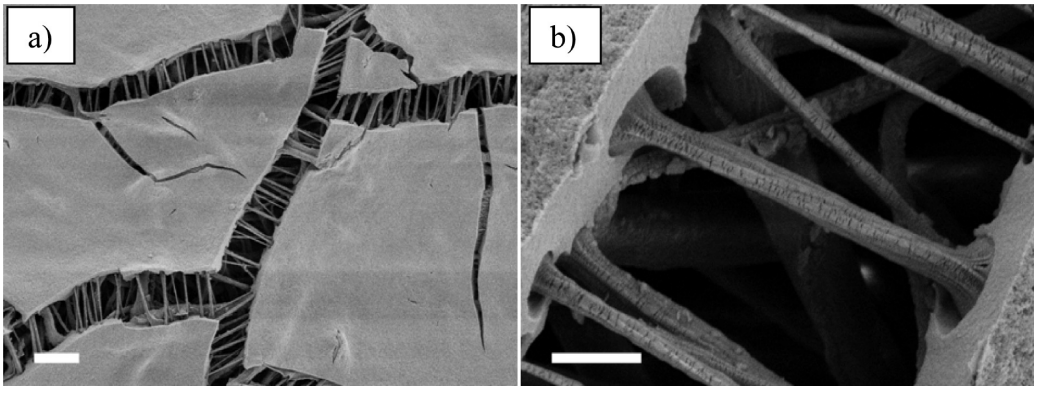

Figure 6. SEM images of $CaCO_3$ films with incorporated (b) PCL meshes. An ACC paste stabilized by PAA (M_w = 2 kg/mol) infiltrated the electrospun PCL nanofiber network by vacuum-assisted means, Aging time, ~ 20 min. Scale bars: (a) 10 μm and (b) 2 μm.

DOI: 10.1021/acs.langmuir.6b02536
Langmuir 2016, 32, 8951−8959

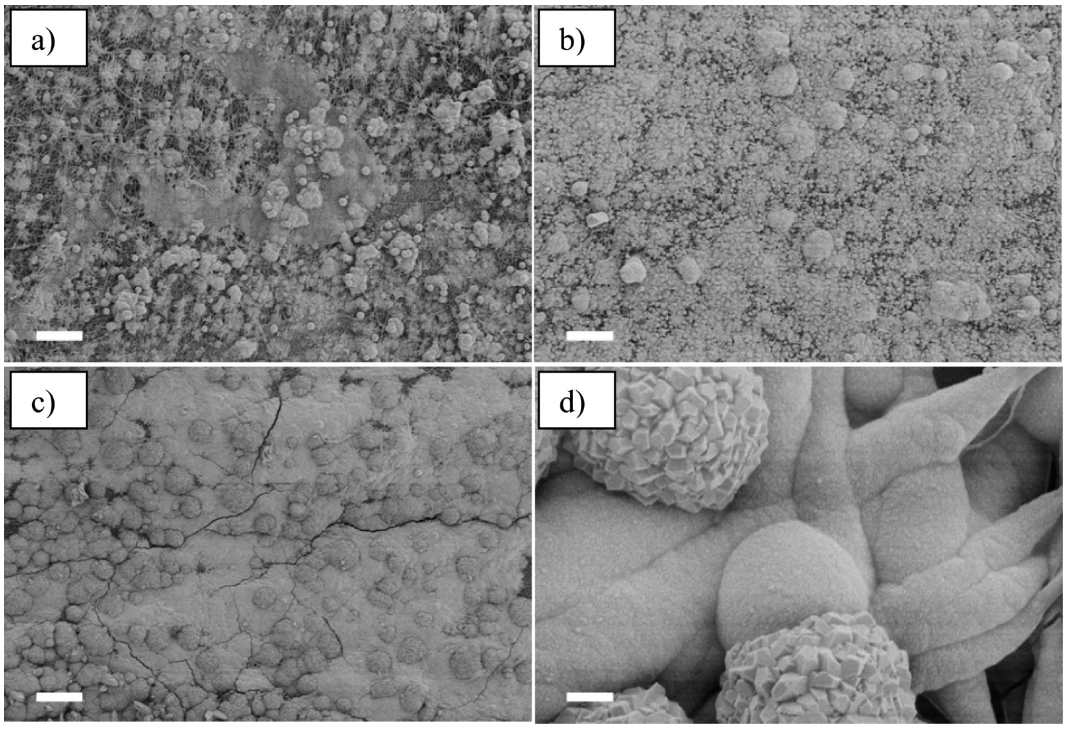

Figure 7. SEM images showed an increased $CaCO_3$ coating on the PCL fiber meshes with increasing crystallization time using PAA as an ACC stabilizer by means of GD. Conditions: $CaCl_2$ = 25 mM, ACC = 50 mM for (a) 1, (b, d) 4.5, and (c) 7 days. Scale bars: (a–c) 100 μm and (d) = 2 μm.

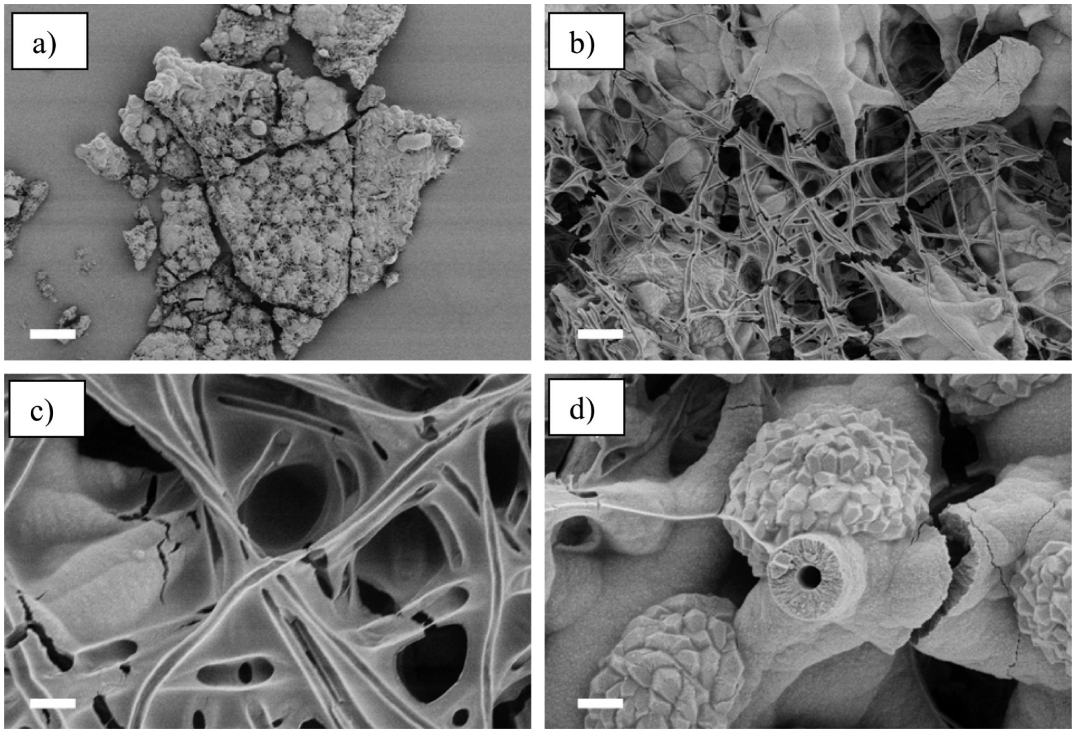

Figure 8. SEM images of $CaCO_3$ demonstrated an intact replica of the PCL fibers upon subsequent leaching (chloroform, 1 day). The sample was crystallized using GD for 4.5 days. Scale bars: (a) 100 μm, (b) = 10 μm, and (c, d) = 2 μm.

coverage of the 0.8 × 0.8 mm^2 fiber meshes. In summary, composite fabrication was successful using different approaches ranging from vacuum-assisted methods to precipitation to GD. It seemed to be promising to use ACC intermediates, and rather highly concentrated solutions were applied for efficient fiber embedding and pore filling of the electrospun fiber meshes rather than direct calcite crystallization at low saturation.

To create porous crystals and to reveal the homogeneity of the coating, the organic fibers were removed. For this purpose, leaching with chloroform and calcination at 500 °C (~10°/min, 3 h dwell time) in an air atmosphere were performed. Leaching of the sample nicely showed the traces of the initial fibers (Figure 8). To some extent, the porous structure of the mesh was retained because the fiber mesh was not completely infiltrated

DOI: 10.1021/acs.langmuir.6b02536
Langmuir 2016, 32, 8951–8959

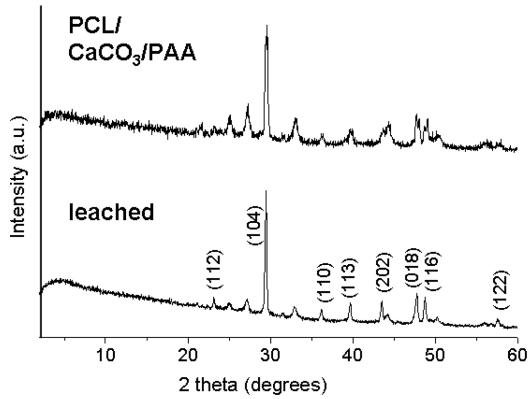

Figure 9. WAXS diffractogram reveals no substantial difference between the composite and the leached $CaCO_3$ body. The main peak suggests mainly calcite crystals.

(i.e., fibers were just partially coated). The resulting porous body could then be fired while maintaining the pore system.

Analyzing the leached $CaCO_3$ body shown in Figure 9 with X-ray diffraction suggested calcite crystals. The main peak at 29.5° 2θ was not accompanied by large neighboring peaks as common for vaterite or aragonite. In addition, most side peaks could be assigned to different calcite crystal planes as indicated by the Miller indices. The remaining small peaks (not tagged) could be attributed to vaterite. Overall, this suggested mainly calcite formation, which is consistent with the SEM images where small calcite-like crystals grow from initially formed ACC particles. In addition, the composite and its leached form showed similar diffractograms. Furthermore, no peak from the PCL fibers is visible, suggesting a large inorganic content, supporting the impressions from the SEM images (Figure 7b,d).

Porous polycrystals or $CaCO_3$/PCL composites were successfully realized, whereas the creation of porous single crystals with dimensions larger than 1 mm seemed to be challenging. Although porous $CaCO_3$ could be interesting for release systems (e.g., drugs), composites might have improved mechanical properties. The mechanical testing (e.g., tensile testing) required a large $CaCO_3$/PCL composite sample area (~3 × 3 cm^2), in addition to a homogeneous inorganic distribution throughout the mesh. Although composite materials were successfully synthesized, the fabrication of larger specimens was not fully realized because the mesh interpenetration or incorporation of $CaCO_3$ was not complete.

For the crystallization of $CaCO_3$ using the GD method, several chemical structures of CNT fibers were used as illustrated in Figure 10.

We used MWCNT functionalized with sulfonic (CNT-2, CNT-3) and carboxylic acid (CNT-5) groups in GD experiments. It is found that both the concentration of $CaCl_2$ solutions and the presence of acidic groups on the MWCNTs backbone have a strong influence on the crystallization behavior, polymorph occurrence, and morphology of the $CaCO_3$ crystals. The CNT fiber concentration, functionalization, and the experimental conditions are crucial to controlling the $CaCO_3$ crystal morphology and the incorporation of these nanofibers into the $CaCO_3$ crystal surface (Figure S.I.4 of the Supporting Information).

In addition, LM images show the formation of a $CaCO_3$ crystal with a black surface appearance indicating CNT fibers incorporation into the crystals as an additive by the GD method; this is shown at 35 min for the different CNTs and different Ca^{2+} concentrations (Figure S.I.5 of the Supporting Information).

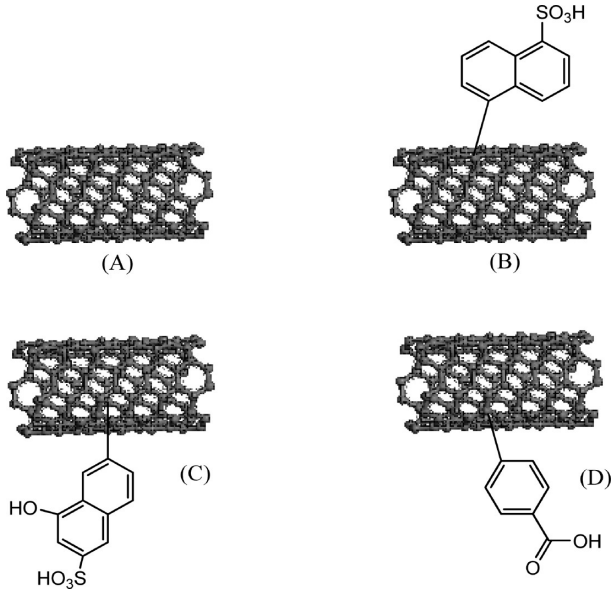

Figure 10. Chemical structures of CNTs: (A) Raw multiwall CNT-1, (B) CNT-2, (C) CNT-3, and (D) CNT-5.

Figure S.I.5 (a1−a3) shows $CaCO_3$ crystals with raw MWCNT (CNT-1) fibers obtained with different $CaCl_3$ concentrations from 5 to 25 mM. In general, these crystals showed rhombohedral calcite with selective CNT fiber deposition on the $CaCO_3$ crystals. However, Figure S.I.5 (b−d) shows different morphologies (truncated, round, and aggregated) of $CaCO_3$ crystals obtained in the presence of functionalized sulfonic acid (CNT-2, CNT-3) and carboxylic acid (CNT-5) CNT fibers as templates. We observed that these $CaCO_3$ crystals lost their well-developed edges and show elongation on the atomic steps of the {104} face. A similar morphology of calcite with stairstep dendritic structures using synthetic peptides and a synthetic organic polymer such as poly(vinyl alcohol) has been reported.[61,62] It is important to mention that in all the cases where CNTs were dispersed in aqueous solution the obtained crystals are black as a result of the presence of CNTs inside the calcite crystal. The incorporation of CNTs inside the $CaCO_3$ particles is an interesting way to introduce new properties (e.g., fluorescent, optical, and electrical) into inorganic crystals.

■ CONCLUSIONS

Electrospun submicrometer fiber meshes and nanosized CNTs were further used for the hybrid fabrication of PCL with $CaCO_3$, a biorelevant mineral. It was possible to incorporate submicrometer-sized plasma-treated PCL meshes with areas >1 mm^2 into $CaCO_3$ using three crystallization methods including the use of PAA. The additive seemed to be useful in stabilizing ACC to effectively fill the space between the electrospun fibers resulting in composite structures. The organic part could be removed by leaching, and the resulting inorganic pore system did not collapse upon a subsequent calcination step. On the other hand, CNT fibers offer a great range for controlled crystallization applications. It was found that differently functionalized CNTs with acidic groups interacted differently with the individual growth planes of $CaCO_3$ crystals using the GD method. The GD method showed that the concentration of functionalized CNT fibers and the experimental crystallization conditions are crucial to controlling the $CaCO_3$ crystal morphology. SEM and LM analysis confirmed that the presence of acidic groups of the

DOI: 10.1021/acs.langmuir.6b02536
Langmuir 2016, 32, 8951−8959

MWCNTs effectively controls the morphogenesis and the crystallographic polymorphism of $CaCO_3$ crystals. Thus, the concentration of soft and/or hard organic templates such as PCL and CNT fibers, the concentration of $CaCl_2$ reactants, and the time were found to be crucial during $CaCO_3$ nucleation and growth. This result confirms that these organic nanofibers based on CNT have a great potential to induce porosity into $CaCO_3$ by direct crystallization processes and to obtain advanced hybrid composite materials with a great potential improvement in properties such as stiffness and bioactivity, as was already shown by SEM analysis. Our suggestion is that at different pH values, functionalized CNT fibers can undergo changes in the charge of the sulfonate or carboxylic acid groups and adopt different orientations in solution and thereby elicit changes in $CaCO_3$ morphology. Therefore, the presence of acidic moieties along the functionalized MWCNT is crucial for interaction with the growing $CaCO_3$ on the nanoscale level, as can also be expected from numerous literature reports on the microscale.[63−66] In summary, we demonstrated that the use of PCL and CNT fibers as an additive or substrate template provides a viable approach for studying various aspects of biomineralization, including the production of controlled particles, soft/hard combined reinforcement, control of porosity, and defined morphologies at microscale and nanoscale levels.

■ ASSOCIATED CONTENT

Supporting Information

The Supporting Information is available free of charge on the ACS Publications website at DOI: 10.1021/acs.langmuir.6b02536.

Additional data from SEM of $CaCO_3$ crystals and $CaCO_3$ films obtained with plasma and PCL meshes as well as light microscopy pictures from the $CaCO_3$/MWCNT and dynamic light scattering (DLS) (PDF)

■ AUTHOR INFORMATION

Corresponding Author

*E-mail: aneira@uchile.cl.

Notes

The authors declare no competing financial interest.

■ ACKNOWLEDGMENTS

This research was supported by a joint program of the Max Planck Society & Fraunhofer Society (MPG-FhG project on bioactive surfaces), the German Research Foundation (DFG, Emmy Noether Program BO 1762/2-3), FONDECYT no. 1140660, and FONDAP ACCDiS no. 15130011 and was funded by Program U-Redes Vicepresidency of Research and Development, University of Chile. PICT 07 02214 (FONCYT, Argentina) César A. Barbero is a permanent research fellow of CONICET (Argentina).

■ ABBREVIATIONS

PCL, poly(ε-caprolactone); MWCNT, multiwalled carbon nanotubes; $CaCO_3$, calcium carbonate; PAA, poly(acrylic acid) solution; GD, gas diffusion; DD, double diffusion; CNT, carbon nanotubes; ACC, amorphous calcium carbonate; WAXS, wide-angle X-ray scattering

■ REFERENCES

(1) Lowenstam, H. A. Minerals from by Organisms. *Science* **1981**, *211*, 1126−1131.

(2) Mann, S. Mineralization in Biological Systems. *Struct. Bonding (Berlin)* **1983**, *54*, 125−174.

(3) Estroff, L. A. Introduction: Biomineralization. *Chem. Rev.* **2008**, *108*, 4329−4331.

(4) Simkiss, K.; Wilbur, K. M. *Biomineralization: Cell Biology and Mineral Deposition*; Academic Press: San Diego, 1989; p 337.

(5) Mann, S.; Webb, J.; Williams, R. J. P. *Biomineralization: Chemical and Biochemical Perspectives*; VCH Verlagsgesellschaft, Weinheim, 1989; p 490.

(6) Mann, S. *Biomineralization Principles and Concepts in Bioinorganic Materials Chemistry*; Oxford University Press: 2001.

(7) Mann, S.; Ozin, G. A. Synthesis of Inorganic Materials with Complex Form. *Nature* **1996**, *382*, 313−318.

(8) Mann, S. The Chemistry of Form. *Angew. Chem., Int. Ed.* **2000**, *39*, 3392−3406.

(9) Lowenstam, H. A.; Weiner, S. *On Biomineralization*; Oxford University Press: New York, 1989.

(10) Kaplan, D.; Adams, W. W.; Farmer, B.; Viney, C. Silk-Biology, Structure, Properties, and Genetics. *Silk Polym. ACS Symposium Series* **1993**, *544*, 2−16.

(11) Mayer, G.; Sarikaya, M. Rigid Biological Composite Materials: Structural Examples for Biomimetic Design. *Exp. Mech.* **2002**, *42*, 395−403.

(12) Mann, S.; Archibald, D. D.; Didymus, J. M.; Heywood, B. R.; Meldrum, F. C.; Wade, V. J. Biomineralization: Biomimetic Potential at the Inorganic-Organic Interface. *MRS Bull.* **1992**, *17*, 32−36.

(13) Bäuerlein, E. Biomineralisation von Einzellern: Eine Auβergewöhnliche Membranbiochemie zur Produktion Anorganischer Nano- und Mikrostrukture. *Angew. Chem.* **2003**, *115*, 636−664.

(14) Rao, A.; Vásquez-Quitral, P.; Fernández, M. S.; Berg, J. K.; Sánchez, M.; Drechsler, M.; Neira-Carrillo, A.; Arias, J. L.; Gebauer, D.; Cölfen, H. pH-Dependent Schemes of Calcium Carbonate Formation in the Presence of Alginates. *Cryst. Growth Des.* **2016**, *16*, 1349−1359.

(15) Wesson, J. A.; Ward, M. D. Pathological Biomineralization of kidney Stones. *Elements* **2007**, *3*, 415−421.

(16) Shchukin, D. G.; Sukhorukov, G. B.; Möhwald, H. Biomimetic Fabrication of Nanoengineered Hydroxyapatite/Polyelectrolyte Composite Shell. *Chem. Mater.* **2003**, *15*, 3947−3950.

(17) Sumper, M.; Brunner, E. Silica Biomineralisation in Diatoms: The Model Organism Thalassiosira pseudonana. *ChemBioChem* **2008**, *9*, 1187−1194.

(18) Zhang, D.-F.; Sun, L.-D.; Zhang, J.; Yan, Z.-G.; Yan, C.-H. Hierarchical Construction of ZnO Architectures Promoted by Heterogeneous Nucleation. *Cryst. Growth Des.* **2008**, *8*, 3609−3615.

(19) Addadi, L.; Weiner, S. Control and Design Principles in Biological Mineralization. *Angew. Chem., Int. Ed. Engl.* **1992**, *31*, 153−161.

(20) Dawlee, S.; Sugandhi, A.; Balakrishnan, B.; Labarre, D.; Jayakrishnan, A. Oxidized Chondroitin Sulfate-Cross-Linked Gelatin Matrixes: A New Class of Hydrogels. *Biomacromolecules* **2005**, *6*, 2040−2048.

(21) Fratzl, P. Biomimetic Materials Research: What can We Really Learn from Nature's Structural Materials? *J. R. Soc., Interface* **2007**, *4*, 637−642.

(22) Bai, H.; Ju, J.; Zheng, Y.; Jiang, L. Functional Fibers with Unique Wettability Inspired by Spider Silks. *Adv. Mater.* **2012**, *24*, 2786−2791.

(23) Meldrum, F. C. Calcium Carbonate in Biomineralisation and Biomimetic Chemistry. *Int. Mater. Rev.* **2003**, *48*, 187−224.

(24) Cölfen, H. Precipitation of Carbonates: Recent Progress in Controlled Production of Complex Shapes. *Curr. Opin. Colloid Interface Sci.* **2003**, *8*, 23−31.

(25) Neira-Carrillo, A.; Vásquez-Quitral, P.; Yazdani-Pdram, M.; Arias, J. L. Crystal Growth of $CaCO_3$ Induced by Monomethylitaconate Grafted Polymethylsiloxane. *Eur. Polym. J.* **2010**, *46*, 1184−1193.

(26) Neira-Carrillo, A.; Yslas, E.; Marini, Y. A.; Vásquez-Quitral, P.; Sánchez, M.; Riveros, A.; Yañez, D.; Cavallo, P.; Kogan, M. J.; Acevedo, D. Hybrid Biomaterials Based on Calcium Carbonate and Polyaniline Nanoparticles for Application in Photothermal Therapy. *Colloids Surf., B* **2016**, *145*, 634−642.

DOI: 10.1021/acs.langmuir.6b02536
Langmuir 2016, 32, 8951−8959

(27) Liang, H.-W.; Liu, S.; Yu, S.-H. Controlled Synthesis of One-Dimensional Inorganic Nanostructures Using Pre-Existing One-Dimensional Nanostructures as Templates. *Adv. Mater.* **2010**, *22*, 3925−3937.
(28) Liu, Y.; Goebl, J.; Yin, Y. Templated Synthesis of Nanostructured Materials. *Chem. Soc. Rev.* **2013**, *42*, 2610−2653.
(29) Liu, Y.-Y.; Liu, L.; Xue, L.; Mao, L.-B.; Gao, H.-L.; Xu, L.; Yu, S.-H. Charged Inorganic Nanowire-Directed Mineralization of Amorphous Calcium Carbonate. *ChemNanoMater.* **2016**, *2*, 259−263.
(30) Weiner, S.; Addadi, L.; Wagner, H. D. Materials Design in Biology. *Mater. Sci. Eng., C* **2000**, *11*, 1−8.
(31) Kim, Y.-Y.; Ganesan, K.; Yang, P.; Kulak, A. N.; Borukhin, S.; Pechook, S.; Ribeiro, L.; Kröger, R.; Eichhorn, S. J.; Armes, S. P.; Pokroy, B.; Meldrum, F. C. An Artificial Biomineral Formed by Incorporation of Copolymer Micelles in Calcite Crystals. *Nat. Mater.* **2011**, *10*, 890−896.
(32) Cho, K. R.; Kim, Y.-Y.; Yang, P.; Cai, W.; Pan, H.; Kulak, A. N.; Lau, J. L.; Kulshreshtha, P.; Armes, S. P.; Meldrum, F. C.; De Yoreo, J. J. Direct Observation of Mineral−Organic Composite Formation Reveals Occlusion Mechanism. *Nat. Commun.* **2016**, *7*, 10187.
(33) Gentsch, R.; Börner, H. G. Designing Three-Dimensional Materials at the Interface to Biology. *Adv. Polym. Sci.* **2010**, *240*, 163−192.
(34) Liu, L.; He, D.; Wang, G.-S.; Yu, S.-H. Bioinspired Crystallization of $CaCO_3$ Coatings on Electrospun Cellulose Acetate Fiber Scaffolds and Corresponding $CaCO_3$ Microtube Networks. *Langmuir* **2011**, *27*, 7199−7206.
(35) Tasis, D.; Tagmatarchis, N.; Bianco, A.; Prato, M. Chemistry of Carbon Nanotubes. *Chem. Rev.* **2006**, *106*, 1105−1136.
(36) Karousis, N.; Tagmatarchis, N.; Tasis, D. Current Progress on the Chemical Modification of Carbon Nanotubes. *Chem. Rev.* **2010**, *110*, 5366−5397.
(37) Chu, H.; Wei, L.; Cui, R.; Wang, J.; Li, Y. Carbon Nanotubes Combined with Inorganic Nanomaterials: Preparations and Applications. *Coord. Chem. Rev.* **2010**, *254*, 1117−1134.
(38) Doyle, C. D.; Rocha, J.-D. R.; Weisman, R. B.; Tour, J. M. Structure-Dependent Reactivity of Semiconducting Single-Walled Carbon Nanotubes with Benzenediazonium Salts. *J. Am. Chem. Soc.* **2008**, *130*, 6795−6800.
(39) Lee, M.; Ku, S. H.; Ryu, J.; Park, C. B. J. Mussel-Inspired Functionalization of Carbon Nanotubes for Hydroxyapatite Mineralization. *J. Mater. Chem.* **2010**, *20*, 8848−8853.
(40) Omori, M.; Watanabe, T.; Tanaka, M.; Okubo, A.; Kimura, H.; Hashida, T. Nanocomposite Prepared from Carbon Nanotubes and Hydroxyapatite Precursors. *Nano Biomedicine* **2009**, *1*, 137−142.
(41) Aryal, S.; Bhattarai, R. R.; K. C, R. B.; Khil, M. S.; Lee, D. R.; Kim, H. Y. Carbon Nanotubes Assisted Biomimetic Synthesis of Hydroxyapatite from Simulated Body Fluid. *Mater. Sci. Eng., A* **2006**, *426*, 202−207.
(42) Gentsch, R.; Boysen, B.; Lankenau, A.; Börner, H. G. Single-Step Electrospinning of Bimodal Fiber Meshes for Ease of Cellular Infiltration. *Macromol. Rapid Commun.* **2010**, *31*, 59−64.
(43) Acevedo, D. F.; Balach, J.; Rivarola, C. R.; Miras, M. C.; Barbero, C. A. Functionalised Conjugated Materials as Building Blocks of Electronic Nanostructures. *Faraday Discuss.* **2006**, *131*, 235−252.
(44) Furniss, B. D.; Hannaford, A. J.; Smith, P. W. G.; Tatchell, A. R. *Vogel's Textbook of Practical Organic Chemistry*, 5th ed.; Prentice Hall: Harlow, 1989.
(45) Xu, A.-W.; Dong, W.-F.; Antonietti, M.; Cölfen, H. Polymorph Switching of Calcium Carbonate Crystals by Polymer-Controlled Crystallization. *Adv. Funct. Mater.* **2008**, *18*, 1307−1313.
(46) Wang, T. X.; Cölfen, H.; Antonietti, M. Nonclassical Crystallization: Mesocrystals and Morphology Change of $CaCO_3$ Crystals in the Presence of a Polyelectrolyte Additive. *J. Am. Chem. Soc.* **2005**, *127*, 3246−3247.
(47) Wang, T. X.; Antonietti, M.; Cölfen, H. Calcite Mesocrystals: "Morphing" Crystals by a Polyelectrolyte. *Chem. - Eur. J.* **2006**, *12*, 5722−5730.
(48) Neira-Carrillo, A.; Pai, R. K.; Fernández, M. S.; Carreño, E.; Vásquez-Quitral, P.; Arias, J. L. Synthesis and Characterization of sulfonated Polymethylsiloxane Polymer as Template for Crystal Growth of $CaCO_3$. *Colloid Polym. Sci.* **2009**, *287*, 385−393.
(49) Neira-Carrillo, A.; Retuert, J.; Martínez, F.; Arias, J. L. Effect of Crosslinked Chitosan as a Constrained Volume on the in vitro Calcium Carbonate Crystallization. *J. Chil. Chem. Soc.* **2008**, *53*, 1367−1372.
(50) Pai, R. K.; Pillai, S. Divalent Cation-Induced Variations in Polyelectrolyte Conformation and Controlling Calcite Morphologies: Direct Observation of the Phase Transition by Atomic Force Microscopy. *J. Am. Chem. Soc.* **2008**, *130* (39), 13074−13078.
(51) Pai, R. K.; Pillai, S. Nanoparticles of Amorphous Calcium Carbonate by Miniemulsion: Synthesis and Mechanism. *CrystEngComm* **2008**, *10*, 865−872.
(52) Weiner, S.; Sagi, I.; Addadi, L. Choosing the Crystallization Path Less Traveled. *Science* **2005**, *309*, 1027−1028.
(53) Addadi, L.; Raz, S.; Weiner, S. Taking Advantage of Disorder: Amorphous Calcium Carbonate and Its Roles in Biomineralization. *Adv. Mater.* **2003**, *15*, 959−970.
(54) Ma, Z.; He, W.; Yong, T.; Ramakrishna, S. Grafting of Gelatin on Electrospun Poly(caprolactone) Nanofibers to Improve Endothelial Cell Spreading and Proliferation and to Control Cell Orientation. *Tissue Eng.* **2005**, *11*, 1149−1158.
(55) Lee, K. L.; Kim, H. Y.; Khil, M. S.; Ra, Y. M.; Lee, D. R. Characterization of Nano-structured Poly(1-caprolactone) Nonwoven Mats via Electrospinning. *Polymer* **2003**, *44*, 1287−1294.
(56) Gentsch, R.; Pippig, F.; Nilles, K.; Theato, P.; Kikkeri, R.; Maglinao, M.; Lepenies, B.; Seeberger, P. H.; Börner, H. G. Modular Approach toward Bioactive Fiber Meshes Carrying Oligosaccharides. *Macromolecules* **2010**, *43*, 9239−9247.
(57) Gentsch, R.; Pippig, F.; Schmidt, S.; Cernoch, P.; Polleux, J.; Börner, H. G. Single-Step Electrospinning to Bioactive Polymer Nanofibers. *Macromolecules* **2011**, *44*, 453−461.
(58) Li, C.; Qi, L. M. Bioinspired Fabrication of 3D Ordered Macroporous Single Crystals of Calcite from a Transient Amorphous Phase. *Angew. Chem., Int. Ed.* **2008**, *47*, 2388−2393.
(59) Loste, E.; Park, R. J.; Warren, J.; Meldrum, F. C. Precipitation of Calcium Carbonate in Confinement. *Adv. Funct. Mater.* **2004**, *14*, 1211−1220.
(60) Oaki, Y.; Kajiyama, S.; Nishimura, T.; Imai, H.; Kato, T. Nanosegregated Amorphous Composites of Calcium Carbonate and an Organic Polymer. *Adv. Mater.* **2008**, *20*, 3633−3637.
(61) Kim, I. W.; DiMasi, E. Identification of Mineral Modulation Sequences within the Nacre-Associated Oyster Shell Protein, n16. *Cryst. Growth Des.* **2004**, *4*, 1113−1118.
(62) Kim, W.; Robertson, R. E. Effects of Some Nonionic Polymeric Additives on the Crystallization of Calcium Carbonate. *Cryst. Growth Des.* **2005**, *5*, 513−522.
(63) Rieger, J.; Thieme, J.; Schmidt, C. Study of Precipitation Reactions by X-ray Microscopy: $CaCO_3$ Precipitation and the Effect of Polycarboxylates. *Langmuir* **2000**, *16*, 8300−8305.
(64) Sedlak, M.; Cölfen, H. Synthesis of Double-Hydrophilic Block Copolymers with Hydrophobic Moieties for the Controlled Crystallization of Minerals. *Macromol. Chem. Phys.* **2001**, *202*, 587−597.
(65) Euliss, L. E.; Bartl, M. H.; Stucky, G. D. Control of Calcium Carbonate Crystallization Utilizing Amphiphilic Block Copolypeptides. *J. Cryst. Growth* **2006**, *286*, 424−430.
(66) Gorna, H.; Muñoz-Espí, R.; Gröhn, F.; Wegner, G. Bioinspired Mineralization of Inorganics from Aqueous Media Controlled by Synthetic Polymers. *Macromol. Biosci.* **2007**, *7*, 163−173.

DOI: 10.1021/acs.langmuir.6b02536
Langmuir 2016, 32, 8951−8959